DMD Fast Forward. Published on July 2, 2022 as DOI: 10.1124/dmd.122.000953
This article has not been copyedited and formatted. The final version may differ from this version.

Transporter-Enzyme Interplay in the Pharmacokinetics of PF-06835919, A First-in-class Ketohexokinase Inhibitor for Metabolic Disorders and Non-alcoholic Fatty Liver Disease

Yan Weng, Kari R. Fonseca, Yi-an Bi, Sumathy Mathialagan, Keith Riccardi, Elaine Tseng, Andrew J. Bessire, Mathew A. Cerny, David A. Tess, A. David Rodrigues, Amit S. Kalgutkar, John Litchfield, Li Di, Manthena V. S. Varma

Pharmacokinetics, Dynamics and Metabolism, Medicine Design, Worldwide R&D, Pfizer Inc, Groton, Connecticut, USA (KA, YB, SM, KR, ET, AB, MC, LD, AD, MV); Pharmacokinetics, Dynamics and Metabolism, Medicine Design, Worldwide R&D, Pfizer Inc, Cambridge, Massacusetts, USA (YW, KF, DT, AK, JL).

DMD Fast Forward. Published on July 2, 2022 as DOI: 10.1124/dmd.122.000953
This article has not been copyedited and formatted. The final version may differ from this version.

Running title: Transporter-enzyme interplay in PK of PF-06835919

Corresponding Author: Manthena V. Varma, Pharmacokinetics, Dynamics, and Metabolism, MS 8220-2451, Pfizer Global Research and Development, Pfizer Inc., Groton, CT 06340; Phone:+1-860-715-0257. Fax: +1-860-441-6402. E-mail: manthena.v.varma@pfizer.com

Number of text pages: 22

Number of Tables: 3

Number of Figures: 4

Number of references: 52

Number of words in Abstract: 248

Number of words in Introduction: 407

Number of words in Discussion: 1636

ABBREVIATIONS: $CL_{int,h}$, intrinsic hepatic clearance; CL_h, plasma hepatic clearance; CYP, cytochrome P450; ECCS, extended clearance classification system; ESF, empirical scaling factor; $f_{u,p}$, fraction unbound in plasma; KHK, ketohexokinase; Kp_{uu}, unbound liver-to-plasma partition coefficient; NASH, non-alcoholic steatohepatitis; OAT, organic anion transporter; OATP, organic anion-transporting polypeptide; P450, cytochrome P450; Q_h, hepatic blood flow; PK, pharmacokinetics; R_{bp}, blood-to-plasma ratio; C_{max}, maximal plasma concentration; T_{max}, time to reach C_{max}; AUC, area under the plasma concentration-time curve; $t_{1/2}$, half-life; HEK, human embryonic kidney cells; PBPK, physiologically-based pharmacokinetic; PHH, plated human hepatocytes.

DMD Fast Forward. Published on July 2, 2022 as DOI: 10.1124/dmd.122.000953
This article has not been copyedited and formatted. The final version may differ from this version.

ABSTRACT

Excess dietary fructose consumption promotes metabolic dysfunction thereby increasing the risk of obesity, type 2 diabetes, non-alcoholic steatohepatitis (NASH), and related comorbidities. PF-06835919, a first-in-class ketohexokinase (KHK) inhibitor, showed reversal of such metabolic disorders in preclinical models and clinical studies, and is under clinical development for the potential treatment of NASH. In this study, we evaluated the transport and metabolic pathways of PF-06835919 disposition and assessed pharmacokinetics in preclinical models. PF-06835919 showed active uptake in cultured primary human hepatocytes, and substrate activity to organic anion transporter (OAT)2 and organic anion transporting-polypeptide (OATP)1B1 in transfected cells. "SLC-phenotyping" studies in human hepatocytes suggested contribution of passive uptake, OAT2- and OATP1B-mediated transport to the overall uptake to be about 15%, 60% and 25%, respectively. PF-06835919 showed low intrinsic metabolic clearance in vitro, and was found to be metabolized via both oxidative pathways (58%) and acyl glucuronidation (42%) by CYP3A, CYP2C8, CYP2C9 and UGT2B7. Following intravenous dosing, PF-06835919 showed low clearance (0.4-1.3 mL/min/kg) and volume of distribution (0.17-0.38 L/kg) in rat, dog and monkey. Human oral pharmacokinetics are predicted within 20% error when considering transporter-enzyme interplay in a PBPK model. Finally, unbound liver-to-plasma ratio (Kp_{uu}) measured in vitro using rat, NHP and human hepatocytes was found to be approximately 4, 25 and 10, respectively. Similarly, liver Kp_{uu} in rat and monkey following intravenous dosing of PF-06835919 was found to be 2.5 and 15, respectively, and notably higher than the muscle and brain Kp_{uu}, consistent with the active uptake mechanisms observed in vitro.

DMD Fast Forward. Published on July 2, 2022 as DOI: 10.1124/dmd.122.000953
This article has not been copyedited and formatted. The final version may differ from this version.

Significance Statement

This work characterizes the transport/metabolic pathways in the hepatic disposition of PF-06835919, a first-in-class KHK inhibitor for the treatment of metabolic disorders and NASH. Phenotyping studies using transfected systems, human hepatocytes and liver microsomes signifies the role of OAT2 and OATP1B1 in the hepatic uptake and multiple enzymes in the metabolism of PF-06835919. Data presented suggest hepatic transporter-enzyme interplay in determining its systemic concentrations and potential enrichment in liver, a target site for KHK inhibition.

DMD Fast Forward. Published on July 2, 2022 as DOI: 10.1124/dmd.122.000953
This article has not been copyedited and formatted. The final version may differ from this version.

INTRODUCTION

Fructose, typically added to foods as table sugar (sucrose: a disaccharide made of glucose and fructose) has become a major ingredient in processed foods due to its perceived sweetness, humectant properties, and low cost. Numerous studies have demonstrated an association between sugar consumption and obesity (Schulze et al., 2004; Palmer et al., 2008), type 2 diabetes (T2D), cardiovascular risk factors (Aeberli et al., 2013), non-alcoholic fatty liver disease (NAFLD) (Abid et al., 2009; Ma et al., 2015), and non-alcoholic steatohepatitis (NASH) (Abdelmalek et al., 2010). While some studies suggest that overconsumption of fructose is pathogenic due to excess caloric intake (Cozma and Sievenpiper, 2014), more recent calorically matched studies demonstrate that fructose overconsumption promotes negative metabolic adaptations in humans such as hyperlipidemia, insulin resistance, steatosis, increased de novo lipogenesis (DNL), cardiovascular risk factors, and visceral adiposity to a greater extent than glucose overconsumption (Schwarz et al., 2017; Taskinen et al., 2017). Ketohexokinase (KHK) is essential for fructose metabolism (converts fructose to fructose-1-phosphate, first-step of the metabolic cascade) as humans with loss-of-function KHK mutations and KHK-null mice fail to metabolize fructose, leading to the accumulation of fructose in plasma and urine (Ishimoto et al., 2012). Upon oral ingestion, fructose is primarily metabolized by the intestines, followed by the liver, pancreas, and kidney (Ishimoto et al., 2012; Jang et al., 2018). Inhibition of KHK has been considered a promising therapeutic hypothesis for the treatment of metabolic diseases supported by studies in KHK-null mice, demonstrating protection from fructose induced hyperlipidemia, insulin resistance, obesity, and NAFLD (Ishimoto et al., 2012; Ishimoto et al., 2013)

DMD Fast Forward. Published on July 2, 2022 as DOI: 10.1124/dmd.122.000953
This article has not been copyedited and formatted. The final version may differ from this version.

PF-06835919 was discovered as a first-in-class KHK inhibitor and has been evaluated in clinical trials for metabolic diseases and NAFLD/NASH (Futatsugi et al., 2020; Gutierrez et al., 2021). PF-06835919 is a highly selective inhibitor of KHK (two isoforms-A/C) in in vitro selectivity assays and showed no development-limiting findings in rat and dog toxicology studies (Futatsugi et al., 2020). In a phase 2 study, KHK inhibition by PF-06835919 lead to reduction in whole liver fat and inflammatory markers and was tolerated in adults with NAFLD (Kazierad et al., 2021). PF-06835919, [(1R,5S,6R)-3-(2-[(2S)-2-Methylazetidin-1-yl]-6-(trifluoromethyl)pyrimidin-4-yl)3-azabicyclo[3.1.0]hex-6-yl]acetic acid, is a low MW (356 Da), high permeability (P_{app} $25x10^{-6}$ cm/s) acid, and is classified as an extended clearance classification system (ECCS) class 1A compound (Varma et al., 2015; Kimoto et al., 2018). Here, we discussed the transport mechanisms and metabolic pathways determining the absorption, distribution, clearance and elimination of this novel agent, PF-06835919, in preclinical species and human.

DMD Fast Forward. Published on July 2, 2022 as DOI: 10.1124/dmd.122.000953
This article has not been copyedited and formatted. The final version may differ from this version.

MATERIALS AND METHODS

Materials

PF-06835919 [(1R,5S,6R)-3-(2-[(2S)-2-Methylazetidin-1-yl]-6-(trifluoromethyl)pyrimidin-4-yl)3-azabicyclo[3.1.0]hex-6-yl]acetic acid and standards of metabolites 373a, 373b, 375a, 375b, 389, and 533 (acyl glucuronide) were obtained from Pfizer Global Material Management (Groton, CT) (Futatsugi et al., 2020). Cyclosporine A, ketoprofen, rifampicin, rifamycin SV were purchased from Sigma-Aldrich (St. Louis, MO). Hepatitis B virus myristoylated-preS1 peptide (HBVpep) was synthesized by New England Peptide (Gardner, MA). Rosuvastatin was purchased from Sequoia Research Products Ltd. (Oxford, UK). [^{3}H]-Taurocholate acid and [^{3}H]-cGMP were purchased from PerkinElmer Life Sciences (Boston, MA). All other compounds were obtained from the Pfizer chemical inventory system.

In Vitro Transport Studies Using Transporter-Transfected cells

HEK293 cells stably transfected with human organic anion transporting-polypeptide (OATP)1B1, OATP1B3, or OATP2B1 were generated at Pfizer Inc. (Sandwich, UK). HEK293 cells stably transfected with human sodium-dependent taurocholate transport protein (NTCP) and organic anion transporter (OAT)2 (functional tv-1 variant) were obtained from the laboratories of Per Artursson (Uppsala University, Sweden) and Ryan Pelis (Dalhousie University, Canada), respectively. HEK293 cells wild-type (WT) and stably transfected with OAT2, OATP1B1, OATP1B3, OATP2B1, or NTCP were seeded at a density of 0.5 to 0.8 $\times 10^5$ cells/well on BioCoat™ 48 or 96-well poly-D-lysine coated plates (Corning Inc., Corning NY), grown in DMEM containing 10% FBS and 1% sodium pyruvate for 48 or 72 h at 37 °C, 90% relative humidity, and 5% CO_2. OATP1B1, OATP1B3, OATP2B1, and NTCP-HEK293 cells were

DMD Fast Forward. Published on July 2, 2022 as DOI: 10.1124/dmd.122.000953
This article has not been copyedited and formatted. The final version may differ from this version.

supplemented with NEAA and GlutaMAX. OAT2-HEK293 cells were supplemented with 1% gentamycin, 1% sodium pyruvate, and 50 µg/ml hygromycin B. Cell culture conditions and experimental procedures are similar to those employed earlier (Bi et al., 2018; Mathialagan et al., 2018).

For the uptake studies, transporter-transfected and WT HEK293 cells were washed three times with warm uptake buffer (HBSS with 20 mM HEPES, pH 7.4) and then incubated with uptake buffer containing compound (0.2 µM) in the absence and presence of inhibitors. Based on our previous studies, ketoprofen showed concentration-dependent inhibition of OAT2 with IC_{50} of ~30 µM, and >80% inhibition at 300 µM (Mathialagan et al., 2018). Therefore, 2 concentrations of ketoprofen in this range were used for inhibition studies. Performance of transporter-transfected cells was validated using in vitro probe substrates: [^{3}H]cGMP (OAT2), [^{3}H]taurocholic acid (OATP1B1), or rosuvastatin (OATP1B3/2B1) as described by Mathialagan et al. (Mathialagan et al., 2018). Cellular uptake was terminated by washing the cells three times with ice-cold transport buffer and then the cells were lysed with 0.1 or 0.2 mL of 1% NP-40 in water (radiolabelled compounds) or methanol containing internal standard (non-labelled compounds). Intracellular accumulation for radiolabelled compounds was determined either by mixing the cell lysate with scintillation fluid followed by liquid scintillation analysis (PerkinElmer Life Sciences, Boston, MA) or by LC-MS/MS analysis for non-labelled compounds containing internal standard CP-628374 in 100% methanol. The total cellular protein content was determined using a Pierce BCA Protein Assay kit (Rockford, IL) according to the manufacturer's specifications. The uptake ratio was calculated as a ratio of accumulation in transfected cells to the accumulation in WT cells at multiple time-points.

DMD Fast Forward. Published on July 2, 2022 as DOI: 10.1124/dmd.122.000953
This article has not been copyedited and formatted. The final version may differ from this version.

Uptake Studies Using Sandwich-culture Human Hepatocytes (SCHH)

Culture conditions for SCHH were described previously (Bi et al., 2006; Bi et al., 2013). Cryopreserved human hepatocytes (Lot HH1025 - female, white, 59 year old) were purchased from In Vitro ADMET Laboratories (Columbia, MD). In short, the cryopreserved human hepatocytes were thawed and seeded (0.35 x10^6 cells/well) into 24-well collagen coated plates using InVitro-HT and InVitro-CP media. The plates were overlaid with 0.25mg/ml matrigel on the second day and the study was conducted on day 5. To determine the uptake clearance and passive diffusion, SCHH were preincubated with or without rifamycin SV (1mM) at 37ºC. The uptake was initiated by the addition of 0.5 ml of 1µM substrate and co-incubated in the same conditions. The reactions were terminated at 0.5, 1, 2 and 5 min by washing the cells three times with ice-cold HBSS buffer. The cells were either lysed with 0.5% Triton-100 for radiolabelled compounds or 100% methanol containing internal standard for non-radiaolabeled compounds. The samples were analyzed by scintillation counting or LC-MS/MS, respectively. The initial uptake rates were calculated by linear fitting (using 0.5-2 min) (Bi et al., 2006; Bi et al., 2013).

Uptake Studies Using Cryopreserved Plateable Human Hepatocytes (PHH)

The hepatic uptake assay was performed using short-term culture primary human hepatocytes as described previously with some modifications (Bi et al., 2017). Cryopreserved human hepatocytes (Lot Hu8246, female, white, 37-year old) were purchased from Thermo Fisher Scientific (Carlsbad, CA). Briefly, cryopreserved hepatocytes were thawed at 37 °C and seeded at a density of 0.35×10^6 cells/well on 24-well collagen I coated plates. The cells were cultured in InVitro-CP media (Celsis IVT, Baltimore, MD) overnight (~18 h). Cells were preincubated with HBSS in the presence or absence of inhibitors for 10 min at 37 °C. The preincubation buffer was

DMD Fast Forward. Published on July 2, 2022 as DOI: 10.1124/dmd.122.000953
This article has not been copyedited and formatted. The final version may differ from this version.

aspirated, and the uptake and inhibition reaction were initiated by adding prewarmed buffer containing compound with or without inhibitors. The reactions were terminated at designated time points (0.5, 1, 2, 5 ***min) by adding ice-cold HBSS immediately*** after removal of the incubation buffer. The cells were washed three times with ice cold HBSS and lysed with 100% methanol containing internal standard. Samples were analysed by LC-MS/MS. Uptake rates were estimated from the initial time-course (typically 0.5-2min) by linear regression. Kinetic parameters of hepatic uptake in human hepatocytes were estimated using the following equation:

$$Uptake\ rate\ = PS_{pd}.C + \frac{V_{max}\ .C}{K_m + C}$$

Where, K_m and V_{max} are active transport affinity and maximum uptake rate, respectively. PS_{pd} is passive clearance, and C is the incubation concentration.

Hepatocyte Relay Method For hepatocyte relay method, PF-06835919 (1 μM) was incubated with human hepatocytes at 2 million cells/mL (Lot DCM , 10 donor pool, BioIVT, Westbury, NY) in the presence and absence of selective CYP and pan-CYP inhibitors with five relays as described previously (Yang et al., 2016).

Metabolite Identification in Hepatocytes across Species

[^{3}H]PF-06835919 (10 μM containing 7.2 μCi, specific activity 480 mCi/mmol) was added to hepatocytes (rat, dog, monkey and human, 0.75 million cells/mL) in a total volume of 1.5 mL. Male Wistar-Han rat hepatocytes (Celsis; product number: M000065; lot DTO), male beagle dog hepatocytes (lot ENI), male cynomolgus monkey hepatocytes (Celsis; lot DNB) and mixed-gender cryopreserved human hepatocytes (Bioreclamation; lot SPB) were used for these studies. Incubations were maintained at 37 °C in incubator set to maintain 85% RH and 5% CO_2. At 0, 2

DMD Fast Forward. Published on July 2, 2022 as DOI: 10.1124/dmd.122.000953
This article has not been copyedited and formatted. The final version may differ from this version.

and 4 h, aliquots (450 µL) were removed and quenched by addition to acetonitrile containing 1% formic acid (2.5 mL). Quenched samples were centrifuged at 1900 xg for 5 min. The supernatant was transferred to clean 15 mL centrifuge tubes and evaporated under nitrogen in a Turbovap (Biotage, Salem, NH) at 30 °C. Concentrated samples were reconstituted in 5:95 acetonitrile:0.1% formic acid in water (150 µL) and analyzed as described below.

Reaction Phenotyping Using Metabolite Formation in Human Liver Microsomes (HLM)

In the reaction phenotyping with metabolite formation study, metabolite standards (373a, 373b, 375a, 375b, and 389) were used to quantify the formation rate of each pathway with and without CYP inhibitors after incubation of PF-06835919 (20 µM) in HLM (0.3 mg/mL, HLM103 pooled lot, Sekisui XenoTech, LLC, Kansas City, KS). Single concentration inhibition studies were performed using the following inhibitors: furafylline (10 µM), 2-phenyl-2-(1-piperdinyl)propane (PPP, 3 µM), montelukast (3 µM), sulfaphenazole (10 µM), n-benzylnirvanol (3 µM), quinidine (1 µM), and ketoconazole (1 µM). The enzymes (CYP3A, CYP2C8 and CYP2C9) that were inhibited were investigated further using multiple inhibitor concentrations and the data were used to calculate f_m.

Reaction Phenotyping with Human Recombinant CYP Enzymes

Each 200 µL incubation contained a single human recombinant CYP (rCYP, 100 pmol/mL) isoform (PanVera, Madison WI and Corning Inc., Corning, NY), or HLM (1 mg/mL) in phosphate buffer (0.1M pH=7.4) containing $MgCl_2$ (3.3 mM), PF-06835919 (10 µM), and NADPH (1.0 mM). Incubations were placed in an incubator set to 37 °C for 1 h. Incubates were protein precipitated with 400 µL of acetonitrile. Precipitated samples were centrifuged for 5 min

DMD Fast Forward. Published on July 2, 2022 as DOI: 10.1124/dmd.122.000953
This article has not been copyedited and formatted. The final version may differ from this version.

at 1800 xg and the supernatants were transferred to clean dolphin-nosed tubes (Analytical Sales and Services, Inc. Flanders, NJ).. Samples were dried using an evaporative centrifuge set to 37 °C. Samples were reconstituted using 100 µL 5:95 acetonitrile:water and analyzed by HPLC/MS.

UGT Reaction Phenotyping

UGT reaction phenotyping was conducted with recombinant UGTs (Corning Life Sciences, Oneonta, NY). and HLM with UGT2B7/2B4 chemical inhibitor 16β-phenyllongifolol (Miners et al., 2021). For the rUGT study, PF-06835919 (10 µM) was incubated with thirteen rUGT (0.5 mg/mL) in the presence of 2% bovine serum albumin (BSA). The acyl glucuronide metabolite formation was monitored, and the UGT clearance was calculated with metabolite standard and relative activity factor (RAF) values (Miners et al., 2021). The UGT isoforms involved in PF-06835919 metabolism were further evaluated in HLM with chemical inhibitor. In the chemical inhibition study, PF-06835919 (20 µM) was incubated with HLM (0.1 mg/mL, 2% BSA) in the presence of 16β-phenyllongifolol-2 (a UGT2B7 and UGT2B4 inhibitor) over a concentration range (0.005 – 50 µM) of inhibitor. The data were used to calculate UGT f_m.

In Vitro Kp_{uu} Determination in Hepatocytes

In vitro Kp_{uu} was determined using suspension hepatocytes in InVitroGRO HI media (Thermo Fisher Scientific, Waltham, MA) supplemented with 4% BSA (bovine serum albumin, fatty acid free, Sigma-Aldrich, St. Louis, MO). Human hepatocytes (Lot DCM, 10 male and female donors), monkey hepatocytes (Lot KNT, 3 male cynomolgus monkey), rat hepatocytes (Lot VSU, 35 male Wistar Han rats) were all purchased from BioIVT (Westbury, NY). The details of the method have been discussed previously (Riccardi et al., 2016; Riccardi et al., 2019; Ryu et

DMD Fast Forward. Published on July 2, 2022 as DOI: 10.1124/dmd.122.000953
This article has not been copyedited and formatted. The final version may differ from this version.

al., 2021). Briefly, PF-06835919 was added to the suspension hepatocytes (0.5 million cells/mL) at 0.1 and 1 μM in the presence of 4% BSA and incubated at 37°C for 4 h on an orbital shaker (150 rpm) in a humidified incubator (75% relative humidity, 5% CO_2/95% air) in duplicate. At the end of the incubation, the samples were centrifuged (500 g, 3 min) and supernatants were sampled for analysis. The remaining media were removed from cells and hepatocytes were washed twice with cold phosphate buffer saline and lysed with mammalian protein extraction reagent (MPER) buffer. An aliquot was sampled for analysis. All the samples were quenched with cold acetonitrile containing internal standard (a cocktail of terfenadine and tolbutamide) and centrifuged. The supernatant was transferred for LC-MS/MS analysis using standard curves from both cells and media. Kp is calculated as the total cell concentration divided by the total media concentration. Binding was measured using HTD96 equilibrium dialysis with device with cellulose membranes (MWCO 12-14K) (HTDialysis, LLC, Gales Ferry, CT) (Riccardi et al., 2019; Ryu et al., 2021). Rat liver homogenate was used as a surrogate of f_{uc} (fraction unbound of cell) as there is no significant species or cell-type difference in cell or tissue binding (Riccardi et al., 2018). Media binding was conducted using 4% BSA in InVitroGRO HI media.

In Vivo Pharmacokinetic and Tissue Kp_{uu} Studies

All procedures performed on the animals were in accordance with regulations and established guidelines and were reviewed and approved by an Institutional Animal Care and Use Committee through an ethical review process. Pharmacokinetic (PK) studies were conducted at BioDuro contract laboratories (Shanghai, China) or at Pfizer labs (Groton, CT). Animals were dosed IV (n=3) at 1 mg/kg and oral (n=2) at 5 mg/kg of PF-06835919. At various time points (e.g., 0, 0.083, 0.25, 0.5, 1, 2, 4, 7 and 24 h), blood samples were taken from which plasma samples were

DMD Fast Forward. Published on July 2, 2022 as DOI: 10.1124/dmd.122.000953
This article has not been copyedited and formatted. The final version may differ from this version.

prepared. For tissue Kp_{uu} studies, rats were dosed with PF-06835919 orally at 0.1, 0.3, 1, 3, 10, and 30 mg/kg, respectively, and sacrificed at 2 h postdose for evaluation of tissue distributions. The tissue Kp_{uu} was calculated as mean of all animals (n=48) as no dose dependent changes were observed. For monkey Kp_{uu} study, animals (n=2) were dosed with PF-06835919 by IV bolus at 1 mg/kg and sacrificed at 6 h postdose for evaluation of tissue distributions. Plasma and tissue homogenate samples were extracted using a protein precipitation method containing internal standard. Samples were centrifuged, and supernatant was quantified using LC-MS/MS. PK data were analyzed using noncompartmental analysis (NCA) in Watson LIMS™ (Thermo Scientific, Philadelphia, PA).

LC/MS/MS Method

DMD Fast Forward. Published on July 2, 2022 as DOI: 10.1124/dmd.122.000953
This article has not been copyedited and formatted. The final version may differ from this version.

LC-MS/MS analysis was performed on a SCIEX Triple Quad 6500 mass spectrometer (SCIEX, Ontario, Canada) equipped with TurboIonSpray interface. The HPLC systems consisted of an Agilent 1290 Infinity binary pump (Agilent Technologies, Santa Clara, CA) and ADDA autosampler (Apricot Designs, Covina, CA and Sound Analytics, Niantic, CT). All instruments were controlled and synchronized by SCIEX Analyst software (version 1.6.2) working in tandem with the ADDA software. Mobile phases were 0.1% formic acid in water (mobile phase A) and 0.1% formic acid in acetonitrile (mobile phase B). The gradient was maintained at 5% B for 0.2 min, followed by a linear increase to 95% B in 0.5 min, and kept at 95% B for 0.3 min then a linear decrease to 5% in 0.02 min. The column was equilibrated at 5% B for 0.5 min. The total run time for each injection was 1.5 min. The chromatographic separation was carried out on a Phenomenex Kinetex C18 100Å 30 × 2.1 mm column with a C18 guard column at a flow rate of 0.8 ml/min. Other fit-for-purpose LC-MS/MS conditions were also used for various studies.

Radiochromatography

For generation of radiochromatographic profiles, the HPLC/UV/MS system described above was utilized, but the column eluent was diverted from the mass spectrometer and directed instead to a PAL HTS-xt fraction collector (Leap Technologies). For each sample, the total column eluent was fractionated in 5-sec intervals and collected in 96-well Scintiplates (Perkin-Elmer) containing a solid scintillant impregnated into the bottom of each well. After collection the plates were transferred to a Genevac vacuum centrifuge for evaporation of the HPLC solvent. The dried plates were then counted using a Microbeta2 plate counter (Perkin-Elmer) measuring tritium β-emission over a 4-min counting time.

DMD Fast Forward. Published on July 2, 2022 as DOI: 10.1124/dmd.122.000953
This article has not been copyedited and formatted. The final version may differ from this version.

Metabolite Identification HPLC/UV/MS/MS Analysis

Samples were analyzed by HPLC/UV/MS/MS using an AB Sciex 6600 Triple-ToF mass spectrometer in conjunction with an Agilent 1290 UHPLC system. A 2.1 x 100 mm, 1.7 µm Acquity CSH Fluoro-phenyl HPLC column (Waters) was heated to 50 °C for separation of analytes. The mobile phase was a gradient of A): water containing 0.1% formic acid, and B): methanol, with a flow rate of 400 µL/min. The mobile phase was maintained at 27% B for 0.5 min, followed by a linear increase to 47% B by 25.5 min, then increased to 90% B by 26.6 min. The column was flushed at 90% B until 27.0 min, then decreased to 27% B by 27.1 min, and was re-equilibrated at 27% B until 30.0 min.UV absorbance was monitored with a photo-diode array detector from 220 – 400 nm. The mass spectrometer was operated in positive-ion mode with a DuoSpray ion source at a potential of 5.5 kV and source heater temperature of 500 °C. The MS collision energy (CE) was set to 10 V, and MS/MS CE was 40 V with a CE spread of 15 V. The declustering potential was 85 V in both cases. Full scan mass spectra were acquired over the range 150 – 1000 m/z with an accumulation time of 200 ms. MS/MS spectra were acquired in an automated fashion based upon the mass defect of PF-06835919 and predicted metabolites using an accumulation time of 100 ms. Mass spectral resolving power was ~40,000 throughout the analysis. Metabolites were characterized by comparisons of mass spectral fragmentation patterns and retention time to synthetic standards of PF-06835919 and previously identified metabolites. All HPLC/UV/MSn data were processed using Peakview v. 2.1.

PBPK modeling and simulations to predict human PK

DMD Fast Forward. Published on July 2, 2022 as DOI: 10.1124/dmd.122.000953
This article has not been copyedited and formatted. The final version may differ from this version.

Whole-body PBPK modeling and simulations of PF-06835919 were performed using population-based ADME simulator, Simcyp (version 20, Certara, Sheffield, UK). The virtual population (10 x10 trials) of healthy subjects with a body weight of ~80 kg and age ranging from 18 to 65 years included both sexes. "Bottom-up" PBPK models – assuming rapid-equilibrium (metabolism-alone) or permeability-limited (transporter-enzyme interplay) for hepatic disposition – were developed using physicochemical properties and in vitro data (Table 4). Methodology adopted in model building is similar to that applied for other transporter substrates (Varma et al., 2013; Varma et al., 2017). Advanced dissolution, absorption, and metabolism (ADAM) model, informed with in vitro permeability data, was adopted to capture intestinal absorption (Fa). With the ADAM model, Fa was predicted to be 100%, which is consistent to the complete absorption noted in rat and dog studies. Full-PBPK model using Rodgers et al. method (default method 2 (Rodgers and Rowland, 2006)) considering rapid equilibrium between blood and tissues was adopted to obtain PF-06835919 distribution into all organs. In parameterizing liver disposition, two scenarios were evaluated: rapid-equilibrium (metabolism-alone) or permeability-limited (transporter-enzyme interplay). For the latter, sinusoidal active uptake and passive diffusion measured in the SCHH studies were employed. Additionally, PK profiles were also simulated using monkey-SSS–derived hepatic clearance as a composite input for human clearance while keeping rest of the PBPK input parameters same as with the 'bottom up' model.

DMD Fast Forward. Published on July 2, 2022 as DOI: 10.1124/dmd.122.000953
This article has not been copyedited and formatted. The final version may differ from this version.

RESULTS

In vitro transport characteristics of PF-06835919 in the transfected cells and primary human hepatocytes

Substrate activity of PF-06835919 (0.2 μM) to hepatic uptake transporters was assessed by measuring its uptake in transporter-transfected and WT-HEK293 cells (Figure 1). PF-06835919 showed transport by OAT2 with uptake ratio (ratio of uptake by OAT2-HEK293 cells to WT-HEK293 cells) of approximately 3-5. Time-dependent uptake in OAT2- and WT-HEK293 cells is presented in Supplementary Figure S1. Additionally, PF-06835919 also showed transport by OATP1B1, while the uptake ratios are ≤1 when tested against OATP1B3 and OATP2B1. Inhibition of OAT2- and OATP1B1-specific transport was noted when using ketoprofen and rifamycin SV as inhibitors, respectively (Figure 1B, 1C and S1).

We investigated the time-dependent uptake of PF-06835919 (1 μM) by human hepatocytes plated in sandwich culture format (SCHH) and short-term plated cultures (PHH). The uptake increased over time and the rates were determined by linear regression of initial datapoints (Figure 2A, Supplementary Figure S2). In SCHH (hepatocyte lot HH1025), the passive diffusion (PS_{pd}) and total uptake clearance were estimated to be about 17.5±3.1 and 54.7±3.0 μL/min/mg-protein following incubations in the absence and presence of 1 mM rifamycin SV, respectively (Bi et al., 2017). Biliary clearance in measured based on cellular accumulation in the presence of transport buffer and Ca^{++}-free buffer was found to be negligible (<0.5 μL/min/mg-protein). PF-06835919 showed concentration-dependent uptake in PHH (hepatocyte lot Hu8246), with active transport characterized by K_m and V_{max} values of 1.4±0.5 μM and 52.1±4.3 pmol/min/mg-protein, respectively (Figure 2B). Further, the effect of various

DMD Fast Forward. Published on July 2, 2022 as DOI: 10.1124/dmd.122.000953
This article has not been copyedited and formatted. The final version may differ from this version.

SLC inhibitors on the transport of PF-06835919 (0.5 μM) was assessed in PHH using our previously reported "SLC-phenotyping" protocols (Bi et al., 2019). OATPs inhibitors, cyclosporine (10 μM) and rifamycin SV (20 μM), significantly reduced PF-06835919 uptake (Figure 2D). Ketoprofen, an OAT2 inhibitor (Mathialagan et al., 2018), showed a marked reduction in the uptake. Additionally, NTCP-selective inhibitor, HBV peptide (König et al., 2014; Yan et al., 2014), did not inhibit PF-06835919 transport. Finally, rifamycin SV, a pan-SLC inhibitor at 1 mM (Bi et al., 2017), reduced PF-06835919 transport by >80% in PHH. Collectively, OAT2 and OATP1B1 were found to play a prominent role in the uptake of PF-06835919 by human hepatocytes. Percent contribution of passive uptake, OAT2- and OATP1B-mediated transport to the overall uptake in hepatocytes in vitro was estimated to be about 15%, 60% and 25%, respectively.

In vitro and in vivo unbound tissue-to-plasma partition coefficient (Kp_{uu})

In vitro Kp_{uu} of PF-06835919 was determined using suspension hepatocytes in the presence of 4% BSA. The method has been shown previously to have good correlation with in vivo liver-to-plasma Kp_{uu} for preclinical species and human (Riccardi et al., 2017; Di et al., 2021). The in vitro Kp_{uu} results of PF-06835919 in rat, monkey and human are summarized in Table 1 along with the in vivo Kp_{uu} data from rat and monkey following intravenous dosing. Liver Kp_{uu} values are above unity in rat (~2.5) and monkey (~15) suggesting active uptake mechanism in vivo. In contrast to liver Kp_{uu}, in vivo Kp_{uu} values are much lower in kidney, muscle and brain further substantiating liver enrichment. In vivo Kp_{uu} in monkey was measured at a single time point of 6 hour. At this time point, the compound is approaching terminal phase following IV dosing (Supplementary Figure S3), and therefore the measured Kp_{uu} is a good approximation of steady-state value. Since terminal phase was not fully achieved, the measured Kp_{uu} is likely lower than

DMD Fast Forward. Published on July 2, 2022 as DOI: 10.1124/dmd.122.000953
This article has not been copyedited and formatted. The final version may differ from this version.

steady state Kp_{uu}. In general, good agreement in the in vitro versus in vivo liver Kp_{uu} values was noted in case of rat and monkey.

In Vitro Metabolism of PF-06835919

In vitro metabolic rate of PF-06835919 was determined in human hepatocytes using the hepatocyte relay method (Yang et al., 2016). The unbound intrinsic clearance is 4.2 mL/min/kg. The metabolic profile of PF-06835919 in hepatocytes is shown in Figure 3. Both oxidative and glucuronide metabolites were observed in human hepatocytes and all in vitro metabolites identified in human were present in the preclinical species including rat, dog, and monkey (Table 3). Three metabolites including acid m/z 389, ketone m/z 373b and glucuronide m/z 533 each accounted for >20% of total radioactivity on ^{3}[H]PF-06835919 incubations with human hepatocytes. In addition, all in vitro human metabolites were present in the plasma of dogs (toxicology species) and most of the metabolites, except for 379d, were also present in plasma of rats (toxicology species) (data not shown). The formation of metabolites of PF-06835919 was investigated with a panel of recombinant human CYP (rCYP) enzymes. The ketone metabolite m/z 373b was detected by LC/UV in rCYP enzymes 1A1, 1A2, 2C8, 2C9, 2C19, 2D6, 3A4, 3A5, and 3A7. The aldehyde metabolite m/z 373a was detected on rCYPs 1A1, and 3A7 incubations, while the primary alcohol m/z 375a was only observed when using rCYP 1A1. No other metabolites were observed by LC/UV.

As PF-06835919 is a low clearance compound, reaction phenotyping was investigated using multiple approaches: hepatocyte relay method (Yang et al., 2016), metabolite formation and human recombinant CYP (rCYP) and UGT enzymes (rUGT) (Di, 2017). Based on metabolite formation rates in human hepatocytes using metabolite standards, PF-06835919 is metabolized by both CYPs (58%) and UGTs (42%). Metabolite formation studies in HLMs indicate that the

DMD Fast Forward. Published on July 2, 2022 as DOI: 10.1124/dmd.122.000953
This article has not been copyedited and formatted. The final version may differ from this version.

predominant CYPs involved in PF-06835919 metabolism are CYP3A (f_m 0.24), CYP2C8 (f_m 0.21) and CYP2C9 (f_m 0.11). The major UGT for PF-06835919 acyl glucuronidation is UGT2B7 (f_m 0.38). Other CYPs and UGTs may also contribute minorly to PF-06835919 metabolism accounting to ~ 3%. The methods used for reaction phenotyping here are state-of-the-art and was shown to reliably define f_m (Di, 2017). Overall, metabolism of PF-06835919 in human involves multiple drug metabolizing enzymes with contribution by any specific CYP enzymes being less than 25%, suggesting low victim DDI risk for drug metabolizing enzymes.

Pharmacokinetics of PF-06835919 in rat, dog and monkey

Intravenous plasma clearance (CL) of PF-06835919 was low in rat, dog and monkey with values in the range of ~0.3 to 1.3 mL/min/kg, respectively (Table 2). Volume of distribution at steady-state (V_{ss}) was also consistently low across the species (0.2 to 0.38 L/kg). Consequently, half-life ($t_{1/2}$) was found to be in the range of 3.2 to 11.1 h with monkey showing a longer $t_{1/2}$. Renal excretion of unchanged compound was negligible across species. Similarly, unchanged compound excreted in the bile was found to be minimal (<5% of dose) in a bile-duct cannulate rat model (data not shown). Bioavailability (F) following oral dosing in a suspension formulation showed complete absorption and minimal first-pass extraction in rat and dog. Dog F was found to be higher than 100%, which is possibly due to saturation of clearance mechanisms with the higher oral dose. Overall, PF-06835919 showed low CL and V_{ss} in the range of typical acidic drugs (El-Kattan et al., 2016), and high oral absorption.

Human PK predictions via PBPK based on in vitro and monkey single-species scaling

PF-06835919 plasma concentration-time profiles following oral dosing (50 mg QD) were simulated assuming rapid-equilibrium (metabolism-alone) or permeability-limited (transporter-enzyme interplay) for hepatic disposition via “Bottom-up” PBPK modeling (Simcyp V20,

DMD Fast Forward. Published on July 2, 2022 as DOI: 10.1124/dmd.122.000953
This article has not been copyedited and formatted. The final version may differ from this version.

Certara, Sheffield UK). In vitro metabolism ($CL_{int,app}$) measured using human hepatocytes and transport data (CL_{pd} and CL_{active}) obtained in SCHH experiments were employed directly. V_{ss} was predicted via Rodger-Rowland method (Rodgers and Rowland, 2006), and oral absorption was projected based on in vitro permeability data. All PBPK model parameters and the data source are listed in Table 4. Based on the clinical PK data (Gutierrez et al., 2021), observed $CL_{h,Human}$ was approximated from oral CL (CL/F) across a dose range (10-600 mg) assuming oral absorption is complete and first-pass extract is negligible [i.e., $CL_{h,Human}$ = (Dose/AUC – renal CL) = 0.32 ± 0.04 mL/min/kg]. Direct scaling of metabolic clearance alone, $CL_{int,app}$, underpredicted human oral clearance by about 3-fold (Figure 4). However, permeability-limited liver model accounting for transporter-enzyme interplay predicted human clearance within 25% error. Additionally, PK profiles were also simulated on the basis of monkey hepatic clearance using single-species scaling (monkey-SSS) method previously developed by our group for acidic/zwitterionic drugs (Tess et al., 2020). With monkey-SSS, human CL/F was predicted to be about 0.2 mL/min/kg, which is about 40% lower than the observed mean. Overall, model accounting for transporter-enzyme interplay well described the clinical PK of PF-06835919.

DMD Fast Forward. Published on July 2, 2022 as DOI: 10.1124/dmd.122.000953
This article has not been copyedited and formatted. The final version may differ from this version.

DISCUSSION

PF-06835919 represents a first-in-class selective KHK inhibitor to have entered clinical trials for the treatment of metabolic disorders and NAFLD/NASH (Futatsugi et al., 2020). In early clinical studies, PF-06835919 was found to be safe and well-tolerated in healthy study participants, and dose-dependently increased plasma fructose indicative of KHK inhibition (Gutierrez et al., 2021; Kazierad et al., 2021). The present study characterizes the transport and metabolic pathways involved in the hepatic clearance of PF-06835919, and thus understand the primary drivers to its clinical PK and target tissue exposure. In vitro studies using transporter-transfected cells and primary human hepatocytes provided evidence for OAT2 and OATP1B1 as the membrane transporters involved in the hepatic uptake of PF-06835919. In the liver, PF-06835919 is primarily metabolized by multiple CYPs and UGT2B7 with metabolism by any single CYP contributing to <25%. Collectively, these results suggest that transporter-enzyme interplay determine the hepatic clearance of PF-06835919, and that modulation of one or both pathways due to drug interactions, pharmacogenomics or diseases state may lead to altered systemic and liver exposure.

In transport studies using the transporter-transfected cells, PF-06835919 was found to be a substrate to OAT2 and OATP1B1 with inhibitors blocking specific transport. PF-06835919 also showed active uptake by primary human hepatocytes both in sandwich-culture format (SCHH) and short-term cultures (PHH). Additionally, we studied the impact of a selected set of transporter inhibitors, which inhibit one or multiple uptake transporters under the experimental conditions previously reported by our group (Bi et al., 2019), in an attempt to define the contribution of OAT2 versus OATP1B1 and other transporters to PF-06835919 hepatic uptake. Cyclosporine A (10 μM) and rifamycin SV (20 μM), known inhibitors of OATPs and NTCP at

DMD Fast Forward. Published on July 2, 2022 as DOI: 10.1124/dmd.122.000953
This article has not been copyedited and formatted. The final version may differ from this version.

these concentrations (Li et al., 2014), reduced uptake in human hepatocytes by only about 25%. However, OAT2 inhibitor (ketoprofen) and a pan-SLC inhibitor (rifamycin SV 1 mM) reduced the hepatocyte accumulation by more than 80% (Figure 3). Overall, in vitro SLC-phenotyping studies suggested predominant role of OAT2-mediated transport in the hepatic uptake of PF-06835919 (~60%), with minor contribution from OATP1B1 (~25%). Recent quantitative targeted proteomic studies by Kumar et al. showed that the total abundance and plasma membrane abundance of several SLCs including OATP1B1 and OAT2 are not significantly different between human liver tissue and hepatocytes in plated cultures (PHH and SCHH) (Kumar et al., 2019). This may imply translation of our in vitro findings to in vivo for this substrate drug. However, while the contribution of transporter activity was mapped in vitro using a validated "SLC-phenotyping" approach (Bi et al., 2019), quantitative role of OAT2 and OATP1B1 to uptake clearance in vivo needs to be further defined via clinical testing in DDI or pharmacogenomics studies.

Clinical relevance of OATP1B-mediated uptake mechanisms is well documented after the assessment of PK in *SLCO1B1* genotyped subjects and administration of known OATP1B1 inhibitors (Shitara et al., 2013; Varma et al., 2015). OAT2 is a relatively less studied transporter, and to quantitatively assess its role in uptake clearance of acids warrants further investigation using *in vivo* preclinical (e.g., knock-out animal models) or clinical (e.g., drug interaction with a selective inhibitor or with subjects carrying reduced function *SLC22A7* alleles) studies. Lack of clinically-relevant OAT2 inhibitors may limit clinical assessment of uptake mechanism, however, a DDI study with single-dose rifampicin or cyclosporine can quantify the significance of OATP1B1-mediated transport in PF-06835919 clinical PK.

DMD Fast Forward. Published on July 2, 2022 as DOI: 10.1124/dmd.122.000953
This article has not been copyedited and formatted. The final version may differ from this version.

PF-06835919 is considered highly permeable given its transcellular permeability of ~25x10^{-6}cm/s across cell monolayer systems (MDCK-low efflux cells), typically used to characterize intestinal permeability/absorption (Varma et al., 2012). However, based on the hepatocyte studies with inhibitors, passive uptake was found to be only ~15% of its total uptake. It is now well documented that hepatic uptake (permeability-limited hepatic disposition) plays an important role in the PK and DDIs of several OATP1B substrates including repaglinide, cerivastatin and montelukast, which show high transcellular transport in permeability assays (Shitara et al., 2013; Varma et al., 2015). In a recent study, Eng et al. evaluated 16 high permeability acids/zwitterions and demonstrated the significance of OATP1B-mediated transporter in vitro and in vivo (Eng et al., 2021). Similarly, we infer that permeability-limited hepatic disposition involving OAT2/OATP1B1 plays an important role in hepatic clearance of PF-06835919. The role of active uptake can be further substantiated with high Kp_{uu} values noted in the in vitro rat, monkey and human hepatocytes, as well as the observed high liver Kp_{uu} in rat and monkey in vivo following IV dosing (Table 1). Notably, in vivo Kp_{uu} in liver is several folds higher than in other tissues like muscle in monkey, which is indicative of liver-specific accumulation (Mikkaichi et al., 2015). Based on a previously validated in vitro Kp_{uu} assay which showed good alignment with clinical observations (Riccardi et al., 2017; Di et al., 2021), human liver Kpuu was projected to be up to 10. It is therefore inferred that the OAT2/OATP1B1-mediated uptake contribute to high free liver-to-plasma concentrations (Kp_{uu}), which may contribute to the liver-specific pharmacological and/or toxicological activities. Consequently, modulation in hepatic transporter and metabolic pathways of PF-06835919 may not only alter its systemic PK, but also influence the free target tissue concentrations (Patilea-Vrana and Unadkat, 2016). However, further clinical studies involving imaging techniques such as positron emission

DMD Fast Forward. Published on July 2, 2022 as DOI: 10.1124/dmd.122.000953
This article has not been copyedited and formatted. The final version may differ from this version.

tomography (PET) may be needed to gain further confidence in these findings (Hernández Lozano and Langer, 2020).

Preclinical PK studies suggested low clearance across all three species (rat, dog and monkey), with blood clearance being <5% of hepatic blood flow in the respective species. Additionally, in vitro human hepatocyte relay studies also yielded low intrinsic clearance ($CL_{int,app}$ 0.9 µL/min/million cells). All the preclinical in vitro and in vivo models converged to a low projected total plasma clearance in human <1 mL/min/kg. Consistent to typical acidic drugs, V_{ss} is low across all species, and the values are within range of that predicted by Rodgers and Rowland method (Rodgers and Rowland, 2006) via the full PBPK model while employing compound physiochemical properties. Collectively, the preclinical dataset generated confidence that PF-06835919 could produce adequate exposure following oral dosing in humans. To this end, PBPK model accounting for transporter-enzyme interplay well predicted human CL following oral dose (Figure 4). Reasonable in vitro-in vivo translation with the approach employed here is consistent with the observations made earlier with acidic drugs in ECCS class 1A that showed OAT2-mediated uptake in vitro (Kimoto et al., 2018). In contrast, accounting for metabolic clearance alone assuming rapid-equilibrium model overestimated plasma exposure of PF-06835919. Considering permeability-limited liver model, given the passive transport clearance (CL_{pd}) across basolateral membrane (measured in SCHH) is almost 20-fold higher than measured metabolic clearance ($CL_{int,app}$) (Table 4), sensitivity analysis with PBPK model indicated DDI risk on enzyme inhibition in addition to uptake inhibition (Varma et al., 2013; Patilea-Vrana and Unadkat, 2016; Varma et al., 2017). However, due to contribution from multiple CYPs and UGT2B7, modulating individual enzymes is expected to produce only <25% change in PF-06835919 plasma exposure.

DMD Fast Forward. Published on July 2, 2022 as DOI: 10.1124/dmd.122.000953
This article has not been copyedited and formatted. The final version may differ from this version.

Several methods are available for enzyme reaction phenotyping, including: (1) changes in parent depletion rate with and without selective chemical inhibitors (or antibodies) in liver microsomes and hepatocytes, (2) changes in metabolite formation rate with metabolite standards in the presence and absences of selective chemical inhibitors (or antibodies), (3) parent depletion or metabolite formation in human recombinant enzymes with RAF, ISEF or REF approaches, (4) using radio-labeled material, and (5) correlation method using reagents with different enzyme activities (Zientek and Youdim, 2015; Di, 2017; Miners et al., 2021). For this study, the first four methods were used to estimate fm by CYPs and UGTs. While there are limitations for each phenotyping approach, multiple methodologies adopted for fm assignment in this study (recombinant CYPs, radioactive metabolite scouting and chemical inhibition in human hepatocytes) provided consistent findings that metabolic pathways of PF-06835919 are mediated via CYP3A4/2C8/2C9 and UGT2B7. In vitro reaction phenotyping data need to be further verified in humans using ADME, DDI and/or pharmacogenomic studies.

Allometry exponents of 0.67 and 0.75 are typically used for single species scaling (Mahmood and Balian, 1996). These values, particularly the standard exponent of 0.75 was derived from the observation that basal metabolic rates across species are scaled by body weight with this exponent (Feldman and McMahon, 1983). In our recent study, leveraging a broad set of acid/zwitterion drugs with hepatic disposition via transporter-enzyme interplay, an optimal value for the allometry exponent was found to be 0.50 for monkey-SSS (Tess et al., 2020). This exponent best predicted the human clearance with AFE of 2.2 and about 85% predictions within 3-fold error for a set of 27 compounds that are predominately OAT2/OATP1B substrates. Consistently, clearance prediction for PF-06835919 using monkey-SSS was within 2-fold of the observed total human plasma clearance suggesting its utility in clearance predictions for uptake

DMD Fast Forward. Published on July 2, 2022 as DOI: 10.1124/dmd.122.000953
This article has not been copyedited and formatted. The final version may differ from this version.

transporter substrates. Although the observed intravenous clearance in rat and dog points to a low hepatic extraction, species scaling via these species was not considered in the prospective predictions due to limited prior validation and anticipated implications of relatively large homology differences in transporters and enzymes compared to human isoforms. Species differences in drug transporters and enzymes and implications for translating preclinical findings to humans have been discussed previously (Martignoni et al., 2006; Chu et al., 2013).

In summary, human PK of PF-06835919, a small MW acid being developed for metabolic disorders and NASH, is determined by hepatic transporter-enzyme interplay. Uptake transport is thought to be driven mainly by OAT2 and OATP1B1 based on in vitro studies using transfected cell systems and primary human hepatocytes, while its metabolism is driven by multiple CYPs and UGT2B7. PF-06835919 showed low systemic clearance across preclinical models, which translated reasonably well to low human clearance as verified with the observed data following oral dosing. Finally, consistent with the Kp_{uu} data noted in preclinical animal models, asymmetric distribution of PF-06835919 into the human liver can be inferred, which may influence its pharmacodynamics.

DMD Fast Forward. Published on July 2, 2022 as DOI: 10.1124/dmd.122.000953
This article has not been copyedited and formatted. The final version may differ from this version.

Acknowledgments

The authors wish to thank Karen Atkinson, Christine Orozco, Xing Yang, Mark Niosi, Laurie Tylaska and Mark West for supporting in vitro transport and metabolism studies. The authors also wish to thank William Esler for reviewing and valuable inputs.

DMD Fast Forward. Published on July 2, 2022 as DOI: 10.1124/dmd.122.000953
This article has not been copyedited and formatted. The final version may differ from this version.

AUTHORSHIP CONTRIBUTIONS

Participated in research design: YW, KF, YB, SM, KR, MC, DT, JL, AK, LD, AD, MV

Conducted experiments: YB, SM, KR, ET, AB, MC

Performed data analysis: YW, KF, YB, SM, KR, ET, MC, DT, LD, MV

Wrote or contributed to the writing of the manuscript: YW, KF, YB, SM, KR, ET, AB, MC, DT, JL, LD, AD, AK, MV

DMD Fast Forward. Published on July 2, 2022 as DOI: 10.1124/dmd.122.000953
This article has not been copyedited and formatted. The final version may differ from this version.

References

Abdelmalek MF, Suzuki A, Guy C, Unalp-Arida A, Colvin R, Johnson RJ and Diehl AM (2010) Increased fructose consumption is associated with fibrosis severity in patients with nonalcoholic fatty liver disease. *Hepatology* **51**:1961-1971.

Abid A, Taha O, Nseir W, Farah R, Grosovski M and Assy N (2009) Soft drink consumption is associated with fatty liver disease independent of metabolic syndrome. *J Hepatol* **51**:918-924.

Aeberli I, Hochuli M, Gerber PA, Sze L, Murer SB, Tappy L, Spinas GA and Berneis K (2013) Moderate amounts of fructose consumption impair insulin sensitivity in healthy young men: a randomized controlled trial. *Diabetes Care* **36**:150-156.

Bi Y-a, Lin J, Mathialagan S, Tylaska L, Callegari E, Rodrigues AD and Varma MV (2018) Role of hepatic organic anion transporter 2 in the pharmacokinetics of R-and S-warfarin: In vitro studies and mechanistic evaluation. *Mol Pharm* **15**:1284-1295.

Bi YA, Costales C, Mathialagan S, West M, Eatemadpour S, Lazzaro S, Tylaska L, Scialis R, Zhang H, Umland J, Kimoto E, Tess DA, Feng B, Tremaine LM, Varma MVS and Rodrigues AD (2019) Quantitative Contribution of Six Major Transporters to the Hepatic Uptake of Drugs: "SLC-Phenotyping" Using Primary Human Hepatocytes. *J Pharmacol Exp Ther* **370**:72-83.

Bi YA, Kazolias D and Duignan DB (2006) Use of cryopreserved human hepatocytes in sandwich culture to measure hepatobiliary transport. *Drug Metab Dispos* **34**:1658-1665.

Bi YA, Qiu X, Rotter CJ, Kimoto E, Piotrowski M, Varma MV, Ei-Kattan AF and Lai Y (2013) Quantitative assessment of the contribution of sodium-dependent taurocholate co-transporting polypeptide (NTCP) to the hepatic uptake of rosuvastatin, pitavastatin and fluvastatin. *Biopharm Drug Dispos* **34**:452-461.

Bi YA, Scialis RJ, Lazzaro S, Mathialagan S, Kimoto E, Keefer J, Zhang H, Vildhede AM, Costales C, Rodrigues AD, Tremaine LM and Varma MVS (2017) Reliable Rate Measurements for Active and Passive Hepatic Uptake Using Plated Human Hepatocytes. *AAPS J* **19**:787-796.

Chu X, Bleasby K and Evers R (2013) Species differences in drug transporters and implications for translating preclinical findings to humans. *Expert Opin Drug Metab Toxicol* **9**:237-252.

Cozma AI and Sievenpiper JL (2014) The Role of Fructose, Sucrose and High-fructose Corn Syrup in Diabetes. *Eur Endocrinol* **10**:51-60.

Di L (2017) Reaction phenotyping to assess victim drug-drug interaction risks. *Expert Opinion on Drug Discovery* **12**:1105-1115.

Di L, Riccardi K and Tess D (2021) Evolving approaches on measurements and applications of intracellular free drug concentration and Kp(uu) in drug discovery. *Expert Opin Drug Metab Toxicol* **17**:733-746.

El-Kattan AF, Varma MV, Steyn SJ, Scott DO, Maurer TS and Bergman A (2016) Projecting ADME Behavior and Drug-Drug Interactions in Early Discovery and Development: Application of the Extended Clearance Classification System. *Pharm Res* **33**:3021-3030.

Eng H, Bi YA, West MA, Ryu S, Yamaguchi E, Kosa RE, Tess DA, Griffith DA, Litchfield J, Kalgutkar AS and Varma MVS (2021) Organic Anion-Transporting Polypeptide 1B1/1B3-Mediated Hepatic Uptake Determines the Pharmacokinetics of Large Lipophilic Acids: In Vitro-In Vivo Evaluation in Cynomolgus Monkey. *J Pharmacol Exp Ther* **377**:169-180.

Feldman HA and McMahon TA (1983) The 3/4 mass exponent for energy metabolism is not a statistical artifact. *Respir Physiol* **52**:149-163.

Futatsugi K, Smith AC, Tu M, Raymer B, Ahn K, Coffey SB, Dowling MS, Fernando DP, Gutierrez JA, Huard K, Jasti J, Kalgutkar AS, Knafels JD, Pandit J, Parris KD, Perez S, Pfefferkorn JA, Price DA, Ryder T, Shavnya A, Stock IA, Tsai AS, Tesz GJ, Thuma BA, Weng Y, Wisniewska HM, Xing G, Zhou J and Magee TV (2020) Discovery of PF-06835919: A Potent Inhibitor of Ketohexokinase (KHK) for the

Treatment of Metabolic Disorders Driven by the Overconsumption of Fructose. *J Med Chem* **63**:13546-13560.

Gutierrez JA, Liu W, Perez S, Xing G, Sonnenberg G, Kou K, Blatnik M, Allen R, Weng Y, Vera NB, Chidsey K, Bergman A, Somayaji V, Crowley C, Clasquin MF, Nigam A, Fulham MA, Erion DM, Ross TT, Esler WP, Magee TV, Pfefferkorn JA, Bence KK, Birnbaum MJ and Tesz GJ (2021) Pharmacologic inhibition of ketohexokinase prevents fructose-induced metabolic dysfunction. *Mol Metab* **48**:101196.

Hernández Lozano I and Langer O (2020) Use of imaging to assess the activity of hepatic transporters. *Expert Opin Drug Metab Toxicol* **16**:149-164.

Ishimoto T, Lanaspa MA, Le MT, Garcia GE, Diggle CP, Maclean PS, Jackman MR, Asipu A, Roncal-Jimenez CA, Kosugi T, Rivard CJ, Maruyama S, Rodriguez-Iturbe B, Sánchez-Lozada LG, Bonthron DT, Sautin YY and Johnson RJ (2012) Opposing effects of fructokinase C and A isoforms on fructose-induced metabolic syndrome in mice. *Proc Natl Acad Sci U S A* **109**:4320-4325.

Ishimoto T, Lanaspa MA, Rivard CJ, Roncal-Jimenez CA, Orlicky DJ, Cicerchi C, McMahan RH, Abdelmalek MF, Rosen HR, Jackman MR, MacLean PS, Diggle CP, Asipu A, Inaba S, Kosugi T, Sato W, Maruyama S, Sánchez-Lozada LG, Sautin YY, Hill JO, Bonthron DT and Johnson RJ (2013) High-fat and high-sucrose (western) diet induces steatohepatitis that is dependent on fructokinase. *Hepatology* **58**:1632-1643.

Jang C, Hui S, Lu W, Cowan AJ, Morscher RJ, Lee G, Liu W, Tesz GJ, Birnbaum MJ and Rabinowitz JD (2018) The Small Intestine Converts Dietary Fructose into Glucose and Organic Acids. *Cell Metab* **27**:351-361.e353.

Kazierad DJ, Chidsey K, Somayaji VR, Bergman AJ, Birnbaum MJ and Calle RA (2021) Inhibition of ketohexokinase in adults with NAFLD reduces liver fat and inflammatory markers: A randomized phase 2 trial. *Med* **2**:800-813.e803.

Kimoto E, Mathialagan S, Tylaska L, Niosi M, Lin J, Carlo AA, Tess DA and Varma MVS (2018) Organic Anion Transporter 2-Mediated Hepatic Uptake Contributes to the Clearance of High-Permeability-Low-Molecular-Weight Acid and Zwitterion Drugs: Evaluation Using 25 Drugs. *J Pharmacol Exp Ther* **367**:322-334.

König A, Döring B, Mohr C, Geipel A, Geyer J and Glebe D (2014) Kinetics of the bile acid transporter and hepatitis B virus receptor Na+/taurocholate cotransporting polypeptide (NTCP) in hepatocytes. *Journal of hepatology* **61**:867-875.

Kumar V, Salphati L, Hop C, Xiao G, Lai Y, Mathias A, Chu X, Humphreys WG, Liao M, Heyward S and Unadkat JD (2019) A Comparison of Total and Plasma Membrane Abundance of Transporters in Suspended, Plated, Sandwich-Cultured Human Hepatocytes Versus Human Liver Tissue Using Quantitative Targeted Proteomics and Cell Surface Biotinylation. *Drug Metab Dispos* **47**:350-357.

Li R, Barton HA and Varma MV (2014) Prediction of pharmacokinetics and drug–drug interactions when hepatic transporters are involved. *Clin Pharmacokinetic* **53**:659-678.

Ma J, Fox CS, Jacques PF, Speliotes EK, Hoffmann U, Smith CE, Saltzman E and McKeown NM (2015) Sugar-sweetened beverage, diet soda, and fatty liver disease in the Framingham Heart Study cohorts. *J Hepatol* **63**:462-469.

Mahmood I and Balian JD (1996) Interspecies scaling: predicting clearance of drugs in humans. Three different approaches. *Xenobiotica* **26**:887-895.

Martignoni M, Groothuis GM and de Kanter R (2006) Species differences between mouse, rat, dog, monkey and human CYP-mediated drug metabolism, inhibition and induction. *Expert Opin Drug Metab Toxicol* **2**:875-894.

Mathialagan S, Costales C, Tylaska L, Kimoto E, Vildhede A, Johnson J, Johnson N, Sarashina T, Hashizume K and Isringhausen C (2018) In vitro studies with two human organic anion transporters: OAT2 and OAT7. *Xenobiotica* **48**:1037-1049.

Mikkaichi T, Nakai D, Yoshigae Y, Imaoka T, Okudaira N and Izumi T (2015) Liver-selective distribution in rats supports the importance of active uptake into the liver via organic anion transporting polypeptides (OATPs) in humans. *Drug Metab Pharmacokinet* **30**:334-340.

Miners JO, Rowland A, Novak JJ, Lapham K and Goosen TC (2021) Evidence-based strategies for the characterisation of human drug and chemical glucuronidation in vitro and UDP-glucuronosyltransferase reaction phenotyping. *Pharmacol Ther* **218**:107689.

Palmer JR, Boggs DA, Krishnan S, Hu FB, Singer M and Rosenberg L (2008) Sugar-sweetened beverages and incidence of type 2 diabetes mellitus in African American women. *Arch Intern Med* **168**:1487-1492.

Patilea-Vrana G and Unadkat JD (2016) Transport vs. Metabolism: What Determines the Pharmacokinetics and Pharmacodynamics of Drugs? Insights From the Extended Clearance Model. *Clin Pharmacol Ther* **100**:413-418.

Riccardi K, Li Z, Brown JA, Gorgoglione MF, Niosi M, Gosset J, Huard K, Erion DM and Di L (2016) Determination of unbound partition coefficient and in vitro-in vivo extrapolation for SLC13A transporter-mediated uptake. *Drug Metab Dispos* **44**:1633-1642.

Riccardi K, Lin J, Li Z, Niosi M, Ryu S, Hua W, Atkinson K, Kosa RE, Litchfield J and Di L (2017) Novel method to predict in vivo liver-to-plasma Kpuu for OATP substrates using suspension hepatocytes. *Drug Metab Dispos* **45**:576-580.

Riccardi K, Ryu S, Lin J, Yates P, Tess D, Li R, Singh D, Holder BR, Kapinos B, Chang G and Di L (2018) Comparison of species and cell-type differences in fraction unbound of liver tissues, hepatocytes, and cell lines. *Drug Metab Dispos* **46**:415-421,S411-S414.

Riccardi KA, Tess DA, Lin J, Patel R, Ryu S, Atkinson K, Di L and Li R (2019) A novel unified approach to predict human hepatic clearance for both enzyme- and transporter-mediated mechanisms using suspended human hepatocytes. *Drug Metab Dispos* **47**:484-492.

Rodgers T and Rowland M (2006) Physiologically based pharmacokinetic modelling 2: predicting the tissue distribution of acids, very weak bases, neutrals and zwitterions. *J Pharm Sci* **95**:1238-1257.

Ryu S, Riccardi K, Jordan S, Johnson N and Di L (2021) Determination of Fraction Unbound and Unbound Partition Coefficient to Estimate Intracellular Free Drug Concentration, in *Quantitative Analysis of Cellular Drug Transport, Disposition, and Delivery, Methods in Pharmacology and Toxicology,* (Rosania GR and Thurber GM eds), Springer

Schulze MB, Manson JE, Ludwig DS, Colditz GA, Stampfer MJ, Willett WC and Hu FB (2004) Sugar-sweetened beverages, weight gain, and incidence of type 2 diabetes in young and middle-aged women. *Jama* **292**:927-934.

Schwarz JM, Noworolski SM, Erkin-Cakmak A, Korn NJ, Wen MJ, Tai VW, Jones GM, Palii SP, Velasco-Alin M, Pan K, Patterson BW, Gugliucci A, Lustig RH and Mulligan K (2017) Effects of Dietary Fructose Restriction on Liver Fat, De Novo Lipogenesis, and Insulin Kinetics in Children With Obesity. *Gastroenterology* **153**:743-752.

Shitara Y, Maeda K, Ikejiri K, Yoshida K, Horie T and Sugiyama Y (2013) Clinical significance of organic anion transporting polypeptides (OATPs) in drug disposition: their roles in hepatic clearance and intestinal absorption. *Biopharm Drug Dispos* **34**:45-78.

Taskinen MR, Söderlund S, Bogl LH, Hakkarainen A, Matikainen N, Pietiläinen KH, Räsänen S, Lundbom N, Björnson E, Eliasson B, Mancina RM, Romeo S, Alméras N, Pepa GD, Vetrani C, Prinster A, Annuzzi G, Rivellese A, Després JP and Borén J (2017) Adverse effects of fructose on cardiometabolic risk factors and hepatic lipid metabolism in subjects with abdominal obesity. *J Intern Med* **282**:187-201.

Tess DA, Eng H, Kalgutkar AS, Litchfield J, Edmonds DJ, Griffith DA and Varma MVS (2020) Predicting the Human Hepatic Clearance of Acidic and Zwitterionic Drugs. *J Med Chem* **63**:11831-11844.

Tess DA, Kimoto E, King-Ahmad A, Vourvahis M, Rodrigues AD, Bergman A, Qui R, Somayaji V, Weng Y, Fonseca KR, Litchfield J and Varma MVS (2022) Effect of a Ketohexokinase Inhibitor (PF-06835919) on In Vivo OATP1B Activity: Integrative Risk Assessment Using Endogenous Biomarker and a Probe Drug. *Clin Pharmacol Ther*.

Varma M, Kimoto E, Scialis R, Bi Y, Lin J, Eng H, Kalgutkar A, El-Kattan A, Rodrigues A and Tremaine L (2017) Transporter-Mediated Hepatic Uptake Plays an Important Role in the Pharmacokinetics and Drug–Drug Interactions of Montelukast. *Clin Pharmacol Ther* **101**:406-415.

Varma MV, Gardner I, Steyn SJ, Nkansah P, Rotter CJ, Whitney-Pickett C, Zhang H, Di L, Cram M, Fenner KS and El-Kattan AF (2012) pH-Dependent solubility and permeability criteria for provisional biopharmaceutics classification (BCS and BDDCS) in early drug discovery. *Mol Pharm* **9**:1199-1212.

Varma MV, Lai Y, Kimoto E, Goosen TC, El-Kattan AF and Kumar V (2013) Mechanistic modeling to predict the transporter- and enzyme-mediated drug-drug interactions of repaglinide. *Pharm Res* **30**:1188-1199.

Varma MV, Steyn SJ, Allerton C and El-Kattan AF (2015) Predicting Clearance Mechanism in Drug Discovery: Extended Clearance Classification System (ECCS). *Pharm Res* **32**:3785-3802.

Yan H, Peng B, Liu Y, Xu G, He W, Ren B, Jing Z, Sui J and Li W (2014) Viral entry of hepatitis B and D viruses and bile salts transportation share common molecular determinants on sodium taurocholate cotransporting polypeptide. *Journal of virology* **88**:3273-3284.

Yang X, Atkinson K and Di L (2016) Novel Cytochrome P450 Reaction Phenotyping for Low-Clearance Compounds Using the Hepatocyte Relay Method. *Drug Metab Dispos* **44**:460-465.

Zientek MA and Youdim K (2015) Reaction phenotyping: advances in the experimental strategies used to characterize the contribution of drug-metabolizing enzymes. *Drug Metab Dispos* **43**:163-181.

Footnotes

All authors are full-time employees of Pfizer Inc. The authors have no conflicts of interest that are directly relevant to this study. No funding was received for the work reported here.

DMD Fast Forward. Published on July 2, 2022 as DOI: 10.1124/dmd.122.000953
This article has not been copyedited and formatted. The final version may differ from this version.

Legends for Figures

Figure 1. Substrate activity of PF-06835919 for four hepatic organic anion transporters, measured using transporter-transfected HEK293 cells (A), effect of OAT2 inhibitor ketoprofen on the uptake in OAT2-transfected HEK293 cells (B), and effect of OATP1B1 inhibitor rifamycin SV on the uptake in OATP1B1-transfected HEK293 cells (C). Uptake ratios for transporter-specific positive controls is presented (D). Uptake ratio is defined as ratio of cell accumulation in transfected cells to wild-type cells. Horizontal line depicts uptake ratio of one. Data are presented as mean ± s.d (n= 6-9). Cyclic guanosine 3',5'-cyclic monophosphate (cGMP), taurocholate (TA), and rosuvastatin (Ros) were used as positive controls for the corresponding transporters.

Figure 2. Uptake transport characterization of PF-06835919 in the cultured primary human hepatocytes, SCHH and PHH. A, time-course of accumulation in SCHH in the absence (diamonds) and presence (triangles) of 1mM rifamycin SV. B, contribution of active and passive transport to uptake in SCHH. C, Michalis-Menten kinetics of transporter-mediated uptake estimated using initial linear uptake rates in PHH. Curve and shaded area depict best fit line and 95% confidence interval. D**,** SLC-phenotyping of PF-06835919 in plated human hepatocytes using a panel of transport inhibitors. Open bars show effect of inhibitors on total uptake (% of control), and last bar depicts fraction transported by OAT2, OATP1B1 and passive mechanisms. Percentage contribution was estimated assuming cyclosporine 10 μM and rifamycin SV 20 μM inhibit OATP1B1, HBV peptide inhibit NTCP alone, ketoprofen inhibit OAT2, and rifamycin SV 1mM inhibit all 5 SLCs. Data represent mean ± s.d. (n=3).

Figure 3. Metabolites of PF-06835919 in rat, dog, monkey, and human hepatocytes.

DMD Fast Forward. Published on July 2, 2022 as DOI: 10.1124/dmd.122.000953
This article has not been copyedited and formatted. The final version may differ from this version.

Figure 4. PBPK based prediction of human pharmacokinetics of PF-06835919 using in vitro data or monkey-SSS. A, Hepatic clearance prediction based on in vitro metabolism and transporter data considering rapid-equilibrium (Heps scaling) and permeability-limited (T-E interplay) models. Additionally, prediction based on monkey-SSS is presented. B, PBPK model simulation of PF-06835919 plasma concentration-time profiles under different assumptions for hepatic clearance. Datapoints depict observed mean (closed) and from individual subjects (open) following 50 mg QD dosing in healthy subjects for 14 days (Gutierrez et al., 2021; Tess et al., 2022).

DMD Fast Forward. Published on July 2, 2022 as DOI: 10.1124/dmd.122.000953
This article has not been copyedited and formatted. The final version may differ from this version.

Table 1. In vitro and in vivo liver-to-plasma Kp_{uu} of PF-06835919 in rat, monkey and human.

Species	Concentration (μM)	In Vitro hepatocyte K_{puu} ± SD (n=3)	In Vivo liver K_{puu}	In Vivo kidney K_{puu}	In Vivo muscle K_{puu}	In Vivo brain K_{puu}
Rat	1	4.0 ± 0.2	2.5	1.1	-	0.40
	0.1	4.8 ± 0.3				
Monkey	1	23.1 ± 3.2	15[a]	3.3	0.38	0.20
	0.1	25.7 ± 0.2				
Human	1	7.8 ± 0.8	-	-	-	-
	0.1	10.0 ± 1.6				

In vivo values presented are mean of triplicate or more measurements.

[a.] Kp_{uu} may be slightly underestimated as terminal phase was not fully reached at 6 hours.

DMD Fast Forward. Published on July 2, 2022 as DOI: 10.1124/dmd.122.000953
This article has not been copyedited and formatted. The final version may differ from this version.

Table 2. Summary of pharmacokinetics of PF-06835919 in rat, dog and monkey

Species	Route	Dose (mg/kg)	*CL* (mL/min/kg)	$t_{1/2}$ (h)	V_{ss} (L/kg)	C_{max} (ng/mL)	*AUC* (ng·h/mL)	F (%)
Rat	IV	1 (n=3)	0.36	7.7	0.20	5510	46,700	-
	PO	5 (n=2)	-	5.7	-	24100	222000	95.0
Dog	IV	1 (n=3)	1.3	3.2	0.17	7570	14,600	-
	PO	5 (n=2)	-	3.4	-	31900	159,000	217
Monkey	IV	1 (n=3)	0.72	11.1	0.38	6190	29,000	-

Values presented are means.

DMD Fast Forward. Published on July 2, 2022 as DOI: 10.1124/dmd.122.000953
This article has not been copyedited and formatted. The final version may differ from this version.

Table 3. In vitro metabolism of PF-06835919 incubated in rat, dog, monkey human hepatocytes for 4h.

Metabolite	Description	Synthetic standard	*m/z*	% of total radioactivity			
				Rat	Dog	Monkey	Human
375a	1° Alcohol	Available	375.16	4.7	11	9.0	9.3
375b	2° Alcohol	Available	375.16	17	2.1	6.4	1.8
389	Acid	Available	389.14	32	7.1	17	25
373b	Ketone	Available	373.14	12	15	16	22
373c	Azetidine oxidation	NA	373.14	1.5	4.4	7.4 ⊥	9.3 ⊥
549a, b	Ketone glucuronide	NA	549.18	-	-	⊥	⊥
373d	Fused-ring oxidation	NA	373.15	1.0	40	-	0.3
533	Acyl Glucuronide + migrations	Available	533.18	15	3.4	39	28
Total radioactivity (%)				83	83	96	96

⊥ Measurement contains contribution from *m/z* 373c and also *m/z* 549a,b due to co-eluting peaks. NA- not available.

DMD Fast Forward. Published on July 2, 2022 as DOI: 10.1124/dmd.122.000953
This article has not been copyedited and formatted. The final version may differ from this version.

Table 4. Summary of PBPK model parameters used to predict or simulate plasma concentration-time profiles of PF-06835919.

Parameters	Value	Source
Molecular weight (g/mol)	356.3	
log P (lipophilicity)	3.972	Calculated
Compound Type	Ampholyte (pKa 1, 4.40; pKa 2, 3.58)	Experimental
Blood-to-plasma ratio	0.588	Experimental
Unbound fraction in plasma	0.076 (binding to serum albumin)	Experimental
Absorption Model	ADAM	
Unbound fraction in gut	1.00	Assumed
Permeability MDCK 10^{-6} cm/s)	25.4	Experimental
Fraction absorbed (Fa)	1.00	Predicted, and consistent to animal Fa data
Absorption Scalar	1.83	Scaled with propranolol as calibrator
V_{ss} (L/kg)	0.14, Full PBPK	Rodgers and Rowland model (Rodgers and Rowland, 2006)
Hepatic Clearance variables		
Direct scaling – input as total systemic clearance (mL/min/kg)	0.20 (from monkey-SSS) or 0.32 (form observed human clearance)	Experimental
Hepatocyte scaling - input as Hepatocyte $CL_{int,app}$ (µL/min/million cells)	0.9	Experimental data using human hepatocytes
Transporter-enzyme interplay - Considering permeability-limited liver model (µL/min/million cells)	CL_{active} = 37.2 $CL_{passive}$ = 17.5 CL_{bile} = 0.38 and $CL_{int,app}$ for metabolism	Experimental data using SCHH studies

PBPK modelling was performed in Simcyp V20 (Certara, Sheffield UK). Simulations were based on healthy population model with 10 trial x 10 subjects size. ADAM, advanced dissolution, absorption and metabolism model; V_{ss}, volume of distribution steady-state; Kp, partition coefficient; SSS, single-species scaling.

DMD Fast Forward. Published on July 2, 2022 as DOI: 10.1124/dmd.122.000953
This article has not been copyedited and formatted. The final version may differ from this version.

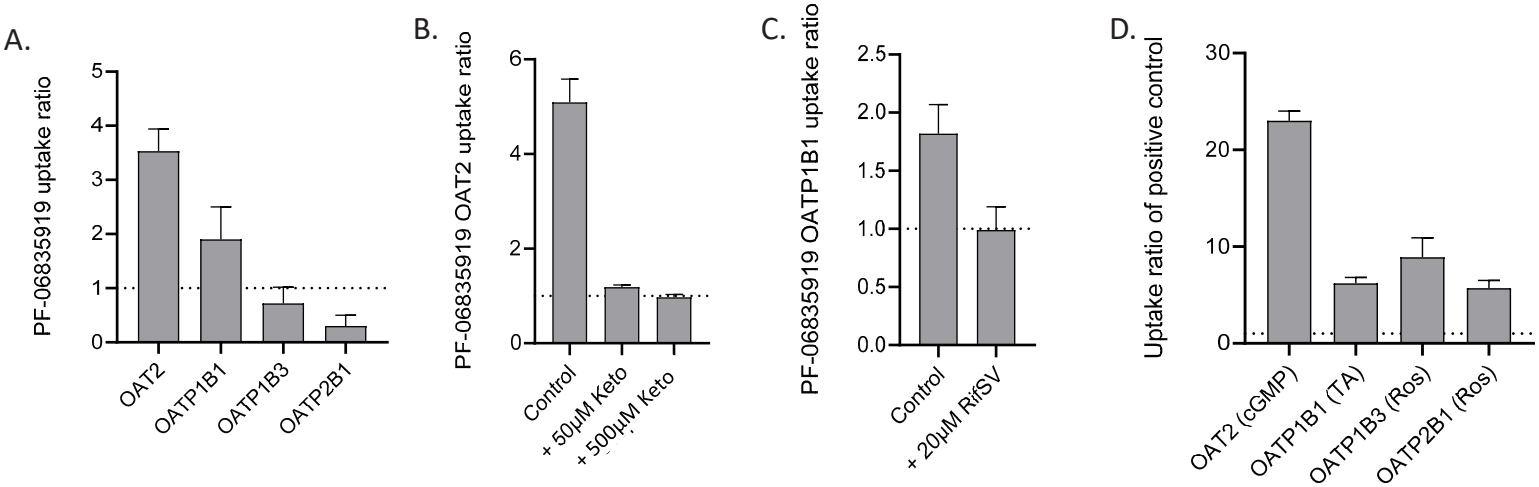

Figure 1.

DMD Fast Forward. Published on July 2, 2022 as DOI: 10.1124/dmd.122.000953
This article has not been copyedited and formatted. The final version may differ from this version.

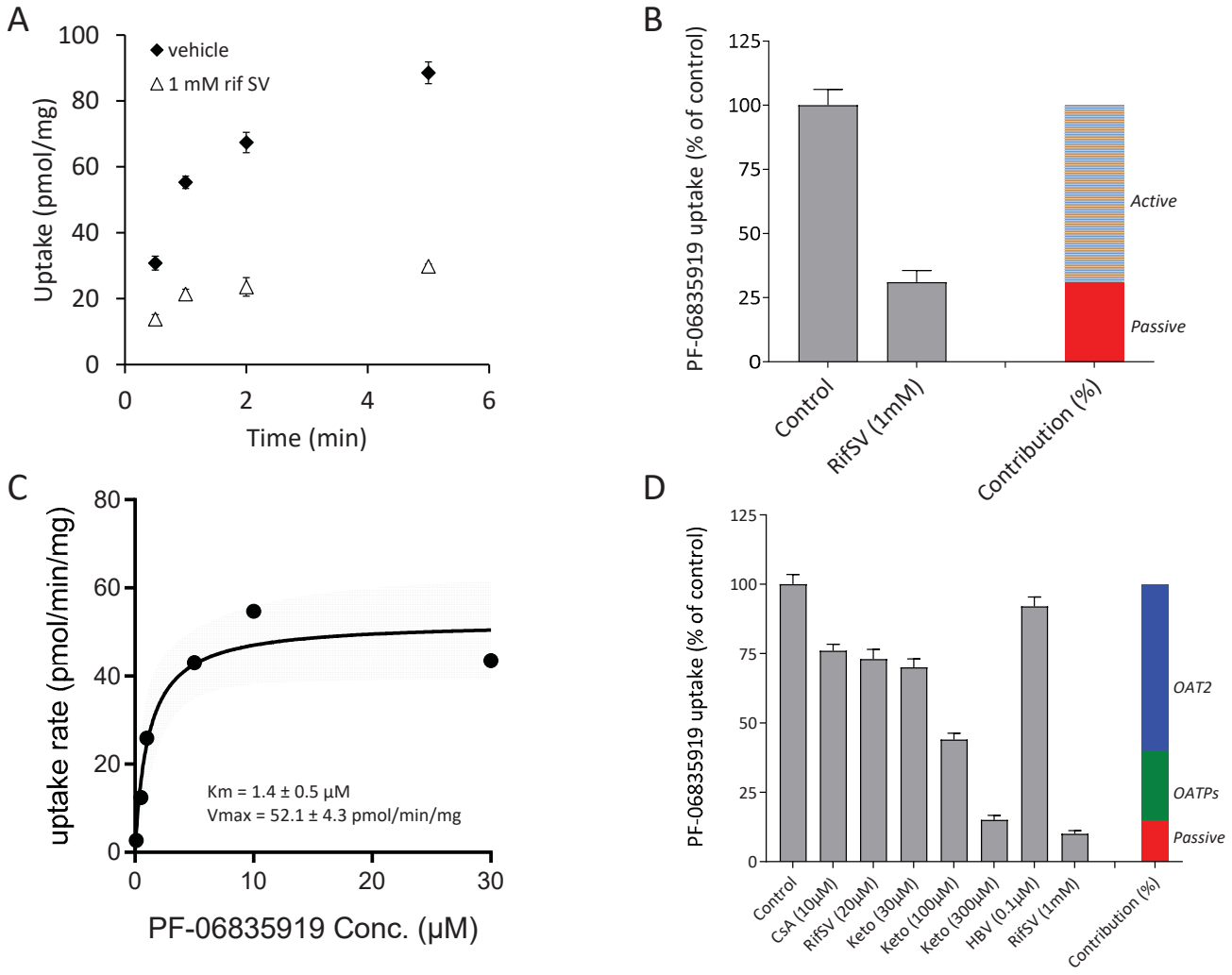

Figure 2.

DMD Fast Forward. Published on July 2, 2022 as DOI: 10.1124/dmd.122.000953
This article has not been copyedited and formatted. The final version may differ from this version.

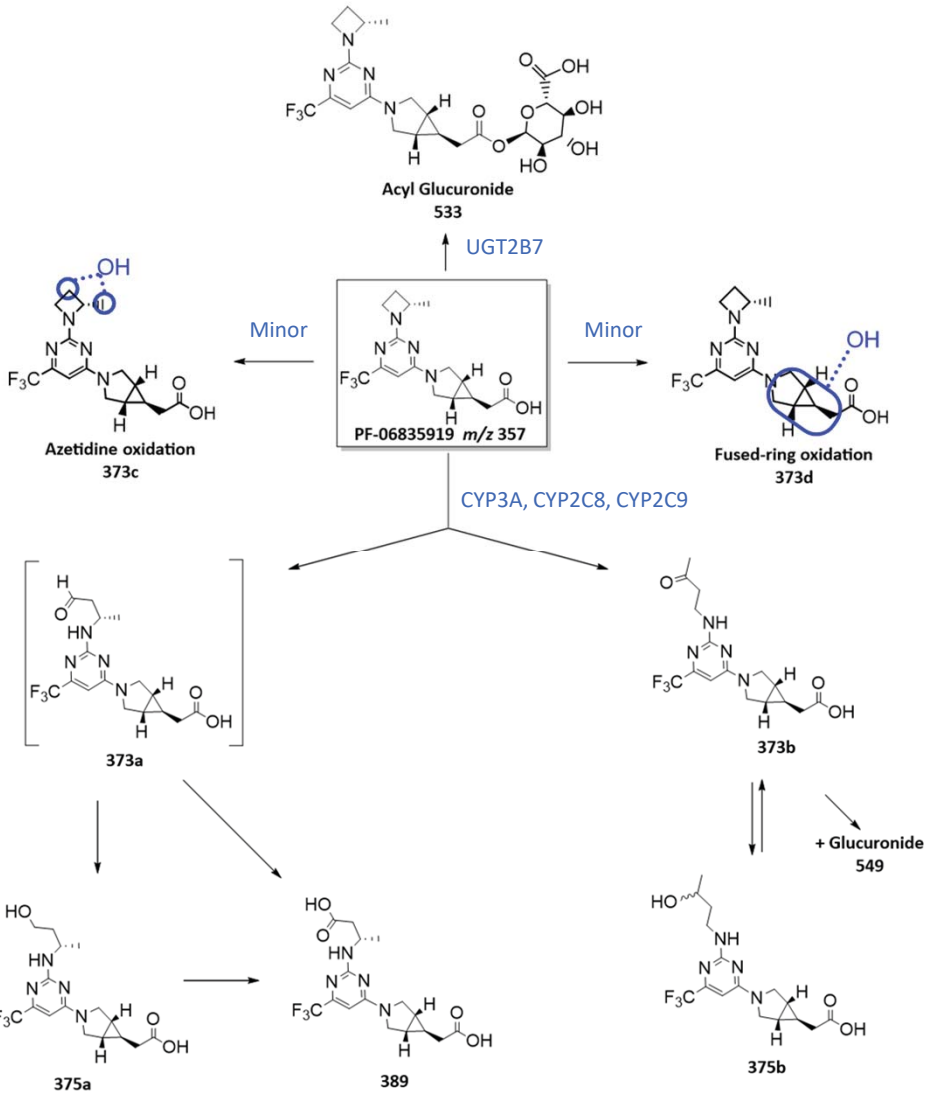

Figure 3.

DMD Fast Forward. Published on July 2, 2022 as DOI: 10.1124/dmd.122.000953
This article has not been copyedited and formatted. The final version may differ from this version.

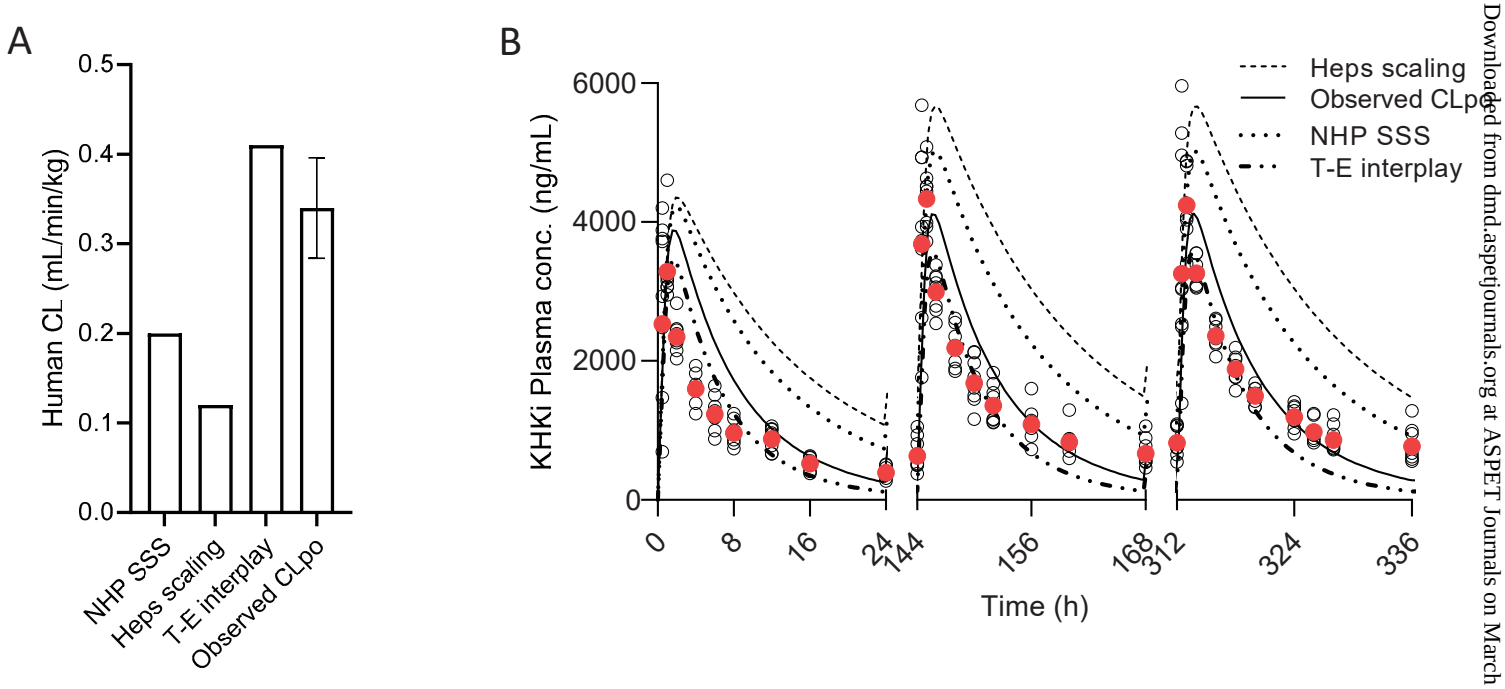

Figure 4.